Directional bleb formation in spherical cells under temperature gradient
Running title: Temperature gradient forms a polar bleb

Kotaro Oyama[1,*], Tomomi Arai[1], Akira Isaka[1], Taku Sekiguchi[1], Hideki Itoh[1,2], Yusuke Seto[1], Makito Miyazaki[1], Takeshi Itabashi[1], Takashi Ohki[1], Madoka Suzuki[3,4,*], and Shin'ichi Ishiwata[1,3,4,*]

[1]Department of Physics, School of Advanced Science and Engineering, Waseda University, 3-4-1 Okubo, Shinjuku-ku, Tokyo 169-8555, Japan
[2]Institute of Medical Biology, Agency for Science, Technology and Research (A*STAR), 8A Biomedical Grove, #06-06 Immunos, Singapore 138648, Singapore
[3]WASEDA Bioscience Research Institute in Singapore (WABIOS), 11 Biopolis Way, #05-02 Helios, Singapore 138667, Singapore
[4]Organization for University Research Initiatives, Waseda University, #304, Block 120-4, 513 Wasedatsurumaki-cho, Shinjuku-ku, Tokyo 162-0041, Japan

K.O., T.A., and A.I. contributed equally to this work.

Present address (K.O. and T.A.): Department of Cell Physiology, The Jikei University School of Medicine, 3-25-8 Nishi-shinbashi, Minato-ku, Tokyo 105-8461, Japan

[*]**Corresponding Authors**
Kotaro Oyama
Department of Physics, School of Advanced Science and Engineering, Waseda University
3-4-1 Okubo, Shinjuku-ku, Tokyo 169-8555, Japan
Tel: +81-3-5286-3437; Fax: +81-3-5286-3437; Email: kou_oyama@akane.waseda.jp

Madoka Suzuki
WASEDA Bioscience Research Institute in Singapore (WABIOS)
11 Biopolis Way, #05-02 Helios, Singapore 138667, Singapore
Tel: +65-6478-9720; Fax: +65-6478-9416; Email: suzu_mado@aoni.waseda.jp

Shin’ichi Ishiwata
Department of Physics, School of Advanced Science and Engineering, Waseda University
3-4-1 Okubo, Shinjuku-ku, Tokyo 169-8555, Japan
Tel: +81-3-5286-3437; Fax: +81-3-5286-3437; Email: ishiwata@waseda.jp

Keywords; Actomyosin, Blebbing, Symmetry breaking, Temperature gradient,

Abstract

Living cells sense absolute temperature and temporal changes in temperature using biological thermosensors such as ion channels. Here, we reveal a novel mechanism of sensing spatial temperature gradients within single cells. Spherical mitotic cells form directional membrane extensions (polar blebs) under sharp temperature gradients (≥ ~0.065°C μm^{-1}; 1.3°C temperature difference within a cell), which are created by local heating with a focused 1455-nm laser beam under an optical microscope. On the other hand, multiple non-directional blebs are formed under gradual temperature gradients or uniform heating. During heating, the distribution of actomyosin complexes becomes inhomogeneous due to a break in the symmetry of its contractile force, highlighting the role of the actomyosin complex as a sensor of local temperature gradients.

Introduction

Temperature-sensitive Ca^{2+} signalling is used by single cells to respond to temporal temperature changes. Transient receptor potential (TRP) channels are representative biological thermosensors in cells (1), but other Ca^{2+} channels such as ryanodine receptor (2), IP_3 receptor (3,4), and Orai1-STIM1 complex (5) also sense temporal temperature changes. This thermosensing function of ion channels is utilized to remotely control neural activity with radio-frequency magnetic-field local heating (6,7). Local heating itself can also induce local gene expression (8), membrane depolarisation (9,10), and muscle contraction (11–13). These local heating techniques have a strong potential for the spatial control of cell functions. However, except for thermotaxis (14–17), biological responses to local temperature gradients remain unclear. *In vitro* studies have revealed that temperature gradients affect cytoskeletal polymerization (18,19), molecular motor activities (20–22), and the distribution of biomolecules including DNA and RNA (23,24), but few studies have observed these biomolecular dynamics in living cells under temperature gradients (25,26). To elucidate the system for sensing temperature gradients, we applied a local temperature gradient to single living cells and observed the directional morphological response coupled with asymmetric protein dynamics.

Materials and Methods

Cell culture.

HeLa cells were cultured in flasks (AGC Techno Glass Co., Shizuoka, Japan) in Dulbecco's Modified Eagle Medium (DMEM) containing 10% foetal bovine serum (FBS), 100 units mL^{-1} penicillin, and 100 μg mL^{-1} streptomycin at 37°C with 5% CO_2. DMEM, FBS, penicillin, and streptomycin were purchased from Thermo Fisher Scientific, Inc. (Waltham, MA, USA). 1–2 days before experiments, cells were seeded on a glass dish (AGC Techno Glass Co.).

Experimental solutions.

Cells on the glass dish were rinsed twice with 1 mL Leibovitz's L-15 medium (Thermo Fisher Scientific, Inc.) containing 10% FBS and incubated in 2 mL L-15 medium containing 10% FBS under the microscope for 15 min at room temperature (25 ± 1°C), at 35 ± 0.5°C or at physiological temperature (37 ± 0.5°C) adjusted by a thermostatically controlled incubator on the sample stage (INUG2-ONICS; Tokai Hit Co., Shizuoka, Japan).

Drug treatments.

Cytoskeleton (actin filament and microtubule) and motor protein (myosin II) inhibitors were mixed into L-15 medium containing 10% FBS 15 min before observation. Actin polymerization was inhibited by 500 nM (final concentration) latrunculin B (Calbiochem, Merck KGaA, Darmstadt, Germany) and 10 μM cytochalasin D (Wako Pure Chemical Industries, Ltd., Osaka, Japan). Actin polymerization was promoted by 50 nM jasplakinolide (Calbiochem). Microtubules were depolymerized with 10 μM nocodazole (Merck KGaA) or stabilized with 20 μM paclitaxel (taxol) (Sigma-Aldrich Co., St. Louis, MO, USA). Myosin II ATPase was inhibited with 100 μM blebbistatin (Toronto Research Chemicals Inc., Ontario, Canada). Rho-kinase (ROCK) and the myosin light chain kinase inhibitors were 10 μM Y-27632 (Wako Pure Chemical Industries, Ltd.) and 20 μM or 50 μM ML-7 (Sigma-Aldrich Co.), respectively. The stock solutions of latrunculin B, cytochalasin D, jasplakinolide, nocodazole, taxol, blebbistatin, Y-27632, and ML-7 were 500 μM, 10 mM, 50 μM, 10 mM, 20 mM, 100 mM, 10 mM, and 20 mM, respectively. Y-27632 was dissolved in sterile water, and the others were dissolved in dimethyl sulfoxide (DMSO) (Sigma-Aldrich Co.). The stock solutions were stored at -20°C. Spherical interphase cells were prepared by rinsing twice with 1 mL phosphate-buffered saline (PBS; 137 mM NaCl, 2.7 mM KCl, 1.5 mM KH_2PO_4, 8.1 mM Na_2HPO_4) containing 0.2 g L^{-1} EDTA and 0.025% trypsin (Thermo Fisher Scientific, Inc.) and incubated for 1 min at 25°C, and the solution was replaced by 2 mL L-15 medium containing 10% FBS for observation.

Optical setup.

The microscope with local heating systems was previously described (11). Confocal fluorescence images were captured with a confocal unit (CSU-X1, Yokogawa Electric Co., Tokyo, Japan), an electron multiplying CCD (EMCCD) camera (iXon-Ultra, Andor Technologies plc, Belfast, Northern Ireland), and an objective lens (PlanApo N 60×/1.45 Oil, Olympus, Tokyo, Japan) attached to the inverted microscope (IX-70, Olympus). The excitation light sources were 488 nm (Sapphire, Coherent Inc., Santa Clara, CA, USA) and 561 nm (Sapphire, Coherent Inc.). The confocal unit was set up with a YOKO-T405/488/561 dichroic mirror (Semrock Inc., Rochester, NY, USA) and YOKO-FF01-520/32 and YOKO-FF01-617/73 emission filters (Semrock Inc.). The excitation and emission light passed through an FF409-Di03 dichroic mirror (Semrock Inc.) in the microscope. Europium (III) thenoyltrifluoroacetonate trihydrate (Eu-TTA), fluorescent beads, blebbistatin, calcein, and ethidium homodimer-1 (EthD-1) were excited by a mercury lamp (Olympus) with excitation filters for Eu-TTA (BP360–370, Olympus) or others (BP470–490, Olympus). Fluo-4 was excited by SPECTRA Light Engine (485/20 nm, Lumencor, Beaverton, OR, USA). For epifluorescence microscopy of Eu-TTA, an FF409-Di03 dichroic mirror (Semrock Inc.) was used. For epifluorescence microscopy of fluorescent beads, blebbistatin, fluo-4, calcein, and EthD-1, a DM505 dichroic mirror (Olympus) and a BA515IF excitation filter (Olympus) were included in the microscope, and fluorescence was observed by epifluorescence microscopy with an EMCCD camera (iXon EM+ 897, Andor Technologies plc) and the same objective lens used for confocal microscopy. Images were captured with iQ (Andor Technologies plc) or in-house software with LabVIEW (National Instruments, Austin, TX, USA).

Temperature measurement generated by infrared laser.

The local temperature around the cell was increased by an infrared laser (λ = 1455 nm, KPS-STD-BT-RFL-1455-02-CO, Keopsys, Lannion, France). The duration of irradiation was controlled by a mechanical shutter (SSH-C4B, Sigma Koki, Tokyo, Japan). Laser power through the objective lens at the specimen position was measured with a thermal disk sensor and a power meter (LM-3 and FieldMaster, Coherent, Inc.). Local temperature changes were calculated from thermal quenching of tetramethylrhodamine (TMR-dextran) or Alexa Fluor 555 (Alexa Fluor 555-dextran) conjugated to 10 kDa dextran (Thermo Fisher Scientific, Inc.). 25 $\mu g\ mL^{-1}$ TMR-dextran or 10 $\mu g\ mL^{-1}$ Alexa Fluor 555-dextran in L-15 medium containing 10% FBS was excited with the 561 nm laser and observed by confocal microscopy. Local temperature changes were also measured with Eu-TTA (Acros Organics, Pittsburgh, PA, USA) in a glass capillary (27). A thin-walled glass capillary (G-100, Narishige Co., Tokyo, Japan) was pulled by a PC-10 puller (Narishige Co.), and the tip was closed by a microforge (MF-900, Narishige Co.). 500 μM Eu-TTA in DMSO was loaded

into the glass capillary by a microloader (Eppendorf AG, Hamburg, Germany). The glass capillary was manipulated by a three-axis motorized micromanipulator (EMM-3NV, Narishige Co.).

The temperature dependence of the fluorescence intensity was measured by a fluorescence spectrophotometer (F-4500, Hitachi High-Technologies Co., Tokyo, Japan) at various temperatures. The temperature in the cuvette was controlled by a precision thermostatic circulator (AB-1600, ATTO Co. Tokyo, Japan) and measured by a digital thermometer (ASF-250T, AS ONE, Osaka, Japan). The excitation and emission wavelengths were, respectively, 555 nm and 578–580 nm for TMR-dextran, 540 nm and 565–568 nm for Alexa Fluor 555-dextran, and 365 nm and 612–618 nm for Eu-TTA. The relative fluorescence intensity of TMR-dextran normalized at 25.1°C was fitted with the quadratic function $y = 1.31\times10^{-4}\ x^2 - 2.47\times10^{-2}\ x + 1.53$, where x and y are the temperature (°C) and normalized fluorescence intensity, respectively (Fig. S1 *A* in the Supporting Material). The fluorescence intensity of Alexa Fluor 555-dextran normalized at 24.9°C was fitted with $y = 2.36\times10^{-4}\ x^2 - 3.66\times10^{-2}\ x + 1.76$ (Fig. S1 *A*), and that of Eu-TTA normalized at 25.1°C was fitted with $y = 3.33\times10^{-4}\ x^2 - 5.17\times10^{-2}\ x + 2.09$ (Fig. S1 *A*). The spatial temperature gradients were fitted with the logarithmic function $y = -a \ln (x/x_0) + b$, where x, x_0, and y were the distance from the heat source (μm), 1 (μm) as a reference, and temperature (°C), respectively (4). The positive numbers a and b were determined with Microsoft Excel. This fitting is based on a model that steady-state temperature distribution $T(r)$ [K] around a cylindrical heat source is described in $T(x_1) = T(x_2) - Q/(2\pi lk) \times \ln(x_1/x_2)$, where x_1 [m] and x_2 [m] are the distances from a center of heat source, Q [W] is a derived power, l [m] is a height of a cylindrical heat source, and k [W m^{-1} K^{-1}] is thermal conductivity of medium. $T(x)$ around a spherical heat source, $T(x_1) = T(x_2) + Q/(4\pi k)\times(1/x_1 - 1/x_2)$, was not well fitted with the spatial temperature gradients measured in this study.

Visualization of actin, myosin, and the cell membrane.

Actin-RFP and tubulin-GFP were expressed by a baculovirus expression system with CellLights (Thermo Fisher Scientific Inc.) one day before observation. F-actin was visualized by Lifeact-RFP (28) or Lifeact-GFP. Myosin II was visualized by mCherry-human myosin, with light chain 2 fluorescently modified (mCherry-MRLC). The plasmids containing Lifeact-RFP, Lifeact-GFP, or mCherry-MRLC were transfected with Lipofectamine LTX (Thermo Fisher Scientific, Inc.) one day before the observation. The plasma membrane was stained with 2.5 μg mL^{-1} CellMask Orange (Thermo Fisher Scientific Inc.) in 2 mL L-15 medium containing 10% FBS for 20 min at 37°C.

Live/dead assay.

To confirm whether bleb-forming cells were alive, we used the LIVE/DEAD Viability/Cytotoxicity Kit (Thermo Fisher Scientific, Inc.). Cells were heated by an infrared laser in HEPES-buffered saline (HBS) (140 mM NaCl, 5 mM KCl, 1 mM $MgCl_2$, 1 mM Na_2HPO_4, 10 mM HEPES, 2 mM $CaCl_2$, 5 mM D(+)-glucose, pH 7.4). To prepare dead cells, cells were incubated in L-15 medium containing 70% methanol for 30 min at room temperature. Both live cells (with or without heating) and dead cells were incubated in HBS containing 2 μM calcein-AM or 4 μM EthD-1 for 15 min at room temperature. The cultures were rinsed twice with 1 mL HBS and incubated in 2 mL HBS, and the fluorescence intensity was measured 1 h after heating.

Visualization of convection flow.

The flow of extracellular solution was visualized with 0.2-μm diameter FluoSpheres Carboxylate-Modified Microspheres (Thermo Fisher Scientific, Inc.) (3). Convection-like water flow was generated by negative pressure produced inside an open-tipped glass capillary placed near a cell. The negative pressure was manually controlled with a syringe pump.

Ca^{2+} imaging.

Fluo-4-AM (Thermo Fisher Scientific, Inc.) was used to observe the intracellular Ca^{2+} dynamics. The cells were incubated in HBS containing 1 μM fluo-4-AM for 30 min at room temperature. The solution was exchanged with HBS for observation. To chelate intracellular Ca^{2+}, cells were incubated in HBS containing 30 μM EGTA-AM (Thermo Fisher Scientific, Inc.) or 50 μM BAPTA-AM (Dojindo Laboratories, Kumamoto, Japan) and 1 μM fluo-4-AM for 30 min at room temperature then observed in Ca^{2+}-free HBS [140 mM NaCl, 5 mM KCl, 1 mM $MgCl_2$, 1 mM Na_2HPO_4, 10 mM HEPES, 5 mM D(+)-glucose, 500 μM EGTA, pH 7.4]. Fluo-4-AM (1 mM), EGTA-AM (30 mM), and BAPTA-AM (50 mM) stocks in DMSO were stored at -20°C. The cells were incubated under the microscope for 15 min before observation to stabilize the temperature. The experiments were completed within 45 min.

Data analysis.

A directional membrane extension was termed a ‘polar bleb’. When organelles inside cells became motionless (Fig. 1 *F*; Movie S7), the state was termed ‘Motionless’. ImageJ (National Institutes of Health, USA) was used for measuring the size of polar blebs. We defined the length and angle of cellular membrane expansion as described below (see also Fig. S2 *A*). We modelled each cell and bleb as a sphere, and defined the circular cell surface before heating (C_0) and the bleb at its maximal extension (C_{bleb}) (see dashed circles in Fig. S2 *A*). A line passing through the centres of C_0 and C_{bleb} was defined as L_C, and the

intersections between L_C and the circular surfaces of the bleb and the cell were, respectively, denoted A and B. The extension length of the membrane, i.e., the size of a polar bleb, was defined as the length of AB. Another line segment connecting the laser heat source with the centre of C_0 was defined as L_L. The expansion angle was defined as the angle between L_C and L_L. A distance from the heat source was defined as the difference between the length of L_L and the radius of C_0.

The actin, myosin, and plasma membrane distributions were measured as the fluorescence intensity of a region of interest (ROI) with ImageJ (Figs. 3 and S12). The change in fluorescence, ΔF, (Figs. 3 *B* and S12) was determined as the difference between the fluorescence intensity 1.7 s after termination of heating and the intensity 0.5 s before heating, F_0. The time course of changes in actin and plasma membrane localization were shown as a series of kymographs (Figs. 4 *B* and S13 *B*). The normalized fluorescence intensities of Lifeact and CellMask (Figs. 4 *C* and S13 *C*) were measured at the black bars shown in the kymographs (Figs. 4 *B* and S13 *B*). The intensity was normalized to the average intensity over 4 s before heating. To observe the dynamics of the cortex, fluorescence images of the cortex were transformed to polar coordinates (Figs. 4 *D* and S11). The profiles start at one intersection of the dashed line through the laser position and the center of the cell (Fig. S11 *A*, gray dashed line) with the cell membrane and then follow the cell contour (Fig. S11 *A*, gray circle) in the cortex region in a clockwise direction. The cell contour was subdivided into 360 points. Then image sequence (Fig. S11 *B*) was obtained from a ROI surrounding the cortex (Fig. S11 *A*, gray rectangle).

The fluorescence intensity of fluo-4 was normalized to the average of intensities for 1 s before heating (F_0). The ROI was set to outline the cell before heating and was changed to accommodate cell movement due to bleb formation. F_{max}/F_0 for a polar bleb was defined as the maximum fluorescence intensity during the first 35 s of heating. F_{max}/F_0 for multiple blebs and 'Motionless' were defined as the maximum fluorescence intensity during the first 50 s of heating.

Statistical analysis.

Extension lengths were compared using Wilcoxon/Mann-Whitney test. The probabilities of forming multiple blebs were compared using Fisher's exact test. The changes in fluorescence intensity of Lifeact-RFP, actin-RFP, and mCherry-MRLC at each side of the cell in the presence of chemical agents were compared to those in the absence of the agent by the following order. First, the variances were compared with the *F*-test. If the variance was equal ($p \geq 0.05$), Student's *t*-test was used. If the difference of variance was statistically significant ($p < 0.05$), Welch's *t*-test was used. To compare the changes in fluorescence intensity between sides, a paired *t*-test was used. Wilcoxon/Mann-Whitney test and Fisher's exact test were performed in OriginPro 9.1 (OriginLab Co., Northampton, MA, USA). All *t*- and

F-tests were performed in Microsoft Excel. Standard error means (SE) are shown for data with statistical analyses; otherwise, standard deviations (SD) are stated.

Results

Polar bleb formation induced by temperature gradient.

We found that a spherical mitotic HeLa cell formed a directional membrane extension (bleb), termed a ‘polar bleb’, under a local temperature gradient created by a focused infrared laser beam (λ = 1455 nm) (Figs. 1, *A–D*, and S1; Movie S1). Bleb formation initiated a few seconds after heating began and continued to expand toward the heat source with strong directionality (Fig. S2). When heating was terminated, expansion stopped, and the bleb slowly shrunk. Upon local heating, 88% (78/89) of spherical metaphase cells formed polar blebs, whereas only 29% (4/14) of interphase cells flattened on the glass surface formed significantly smaller blebs (Fig. S3; Movie S2). However, when the interphase cells were treated with trypsin to induce spherical morphology, 98% (42/43) formed polar blebs during heating (Fig. S3; Movie S3). These results indicate that spherical cells form a polar bleb independent of cell cycle phase. We further confirmed that formation of the polar bleb was not due to convective flow of water (Fig. S4; Movie S4).

Temperature field to induce the polar bleb formation.

Next, we examined various temperature increases (ΔT), at different ambient temperatures before heating (T_0) and temperature differences between the proximal and distal ends of a cell, i.e. the temperature gradient within a cell, toward the heat source (Fig. 1 *C*) by varying the laser power and the distance from the heat source to the cell (Fig. 1 *B*). When cells were heated from 37°C to 42–50°C under a small temperature gradient within a cell (<1.3°C), 84% (59/70) of cells formed multiple sequential, non-directional blebs after re-cooling (Figs. 1 *E* and S5; Movies S5 and S6). During and after heating above ~50°C, organelles inside cells became motionless (Fig. 1 *F*; Movie S7). Hereafter we call this state ‘Motionless’. Sharper temperature gradients induced polar bleb formation at the warmer side of cells with higher probability (Fig. 1, *G–J*). The minimum temperature difference between the ends of a cell required to form a polar bleb was as small as 1.3°C (Fig. 1 *G*), and the absolute temperature ($\Delta T + T_0$) required to induce these responses decreased as T_0 decreased (Fig. S6). These results clearly showed that cell responses depend on ΔT and the spatial temperature gradient. A fluorescent cell viability assay showed that local heating for 20 s does not completely kill the cells within 1 h (100% alive after forming a polar bleb or multiple blebs, 83–86% alive after organelles became motionless), i.e. esterase activity and the plasma membrane are not impaired (Fig. S7). However, even a short pulse of local heating for 5 s increased the probability of normal cytokinesis inhibition for ΔT > 10°C at T_0 = 37°C independent of bleb formation (Fig. S8).

Actomyosin interaction is essential for bleb formation.

Without contacting surrounding cells, the shape of a spherical cell is precisely balanced at the cell periphery by the inward contractile force of cortical actomyosin and the outward hydrostatic pressure on the plasma membrane (29,30). A local imbalance immediately causes blebbing (31,32). Given these properties, what is the thermosensor for the polar bleb formation? Polar blebs were hardly formed in the presence of an actin polymerization inhibitor, i.e., latrunculin B or cytochalasin D (Fig. 2 *A*; Movie S8). In the presence of actin polymerization-promoting drug, jasplakinolide, the length of extrusion was significantly increased. The inhibitor of myosin II ATPase, blebbistatin, also prevented the formation of polar blebs during heating (Figs. 2 *A* and S9), and Y-27632 (rho-kinase inhibitor that indirectly inhibits myosin II) suppressed the formation of polar blebs (Fig. 2 *A*). However, the inhibitor of myosin light chain kinase (MLCK), ML-7, has no significant effect ($p > 0.05$) (Fig. 2 *A*). From these results except for ML-7, we conclude that actomyosin interaction is essential for the formation of polar blebs, which is similar to spontaneous blebbing during cytokinesis, apoptosis, and migration (27,28). We therefore focused on microtubule dynamics and found that nocodazole (microtubule-depolymerizing drug) significantly increased the length of extrusion, whereas taxol (microtubule stabilizer) did not increase the extension length (Fig. 2 *A*). These results suggest that microtubule-supported structures such as the mitotic spindle interfere with bleb extension. Multiple blebs were also suppressed by the inhibitors of actin polymerization and myosin II ATPase (Fig. 2 *B*). 'Motionless' was not affected by these inhibitors (Fig. 2 *C*), suggesting that 'Motionless' is probably attributable to thermal denaturation of proteins.

Temperature-sensitive Ca^{2+} dynamics is not essential for polar bleb formation.

Next, we investigated the effects of the Ca^{2+} increase induced by local heating on bleb formation because Ca^{2+} dynamics is a major response to temperature changes and are expected to disturb the contractile force of actomyosin (Discussion). Under conditions that form polar blebs (T_0 = 25°C, ΔT = 12°C) (Fig. S6), Ca^{2+} bursts were mainly observed immediately after re-cooling and occasionally during heating (Fig. S10, *A* and *B*; Movie S9). The Ca^{2+} burst induced by re-cooling is attributable to breaking the balance of the temperature sensitivities between IP_3 receptors and sarco/endoplasmic reticulum Ca^{2+}-ATPase (SERCA) in the endoplasmic reticulum (ER) (3,4). Under conditions that induce multiple blebs or 'Motionless', the Ca^{2+} bursts generally began during heating. Intracellular Ca^{2+} chelates (EGTA or BAPTA) prevented the Ca^{2+} burst (Fig. S10, *B* and *C*). However, polar bleb formation was not influenced in either EGTA- or BAPTA-loaded cells (Fig. S10 *D*), suggesting that the Ca^{2+} increase during heating was not essential for polar bleb formation (Fig. S10 *A*). However, the probability of multiple bleb formation was significantly decreased by the addition of EGTA or BAPTA, suggesting that Ca^{2+} bursts have some role in the initiation of multiple bleb formation (Fig. S10; Movie S9; see also

Discussion).

Symmetry breaking of actomyosin cortex induced by temperature gradient.

We further investigated the dynamics of the actomyosin cortex with Lifeact-RFP, which specifically binds to actin filaments (F-actin) (28), and actin-RFP expressed in the cell. Under the temperature gradient that induces polar bleb formation, the fluorescence intensities of both Lifeact-RFP and actin-RFP became asymmetric, decreasing and increasing at the near (warmer) and far (cooler) sides of the cell, respectively (Figs. 3, *A* and *B*, S11; Movies S10 and S11). Fluorescence intensities of GFP and RFP decreased when temperature was increased (6,8). Although the thermal quenching of RFP took place during heating, the quenched fluorescence immediately recovered upon recooling because it is a reversible process. Furthermore, in the presence of blebbistatin or Y-27632, the symmetry of actin-RFP was not broken (Fig. 3 *B*), showing that the temperature increase did not cause irreversible decrease in the fluorescence intensity of proteins. These results show that the net decrease in the fluorescence intensity observed after heating is not attributable to the thermal quenching but to irreversible change in the actin cortex density. Larger ΔT values enhanced both the asymmetry and extension length of polar blebs (Fig. S12). The distribution pattern of mCherry-human myosin regulatory light chain 2 (mCherry-MRLC) was similar to that of F-actin (Fig. 3, *A* and *B*; Movie S12). In the presence of blebbistatin, Y-27632, or cytochalasin D, both F-actin and myosin II accumulated less significantly to the cooler side than in non-treated cells, but the decrease in the amount of F-actin at the warmer side still occurred (Fig. 3 *B*; Movies S13, S14, S15). From these results, we conclude that the accumulation of F-actin toward the cooler side is caused by the imbalance of the contractile force of the actomyosin II complex between the warmer and cooler sides (see discussion below). The accumulations of the cortex and membrane toward the cooler side are coupled with polar bleb formation. CellMask-stained plasma membranes showed inhomogeneous localization similar to Lifeact-RFP and actin-RFP (Fig. 3, *A* and *B*; Movie S16). Simultaneous observation of Lifeact-GFP and CellMask revealed that F-actin and the membrane were likely to move together to the cooler side until the bleb was formed (Fig. 4, *A*–*D*; Movie S17). During this rearrangement, a polar bleb began to appear ~3 s after the start of heating (Fig. 4, *A*–*C*). In a small number of cases, we observed that smaller ΔT values also induced a polar bleb without noticeable inhomogeneous distribution of the cortex or with an increase in the cortex at the warmer side (Figs. S12 and S13; Movie S18).

Discussion

Spontaneous bleb formation is reportedly initiated by detachment of the plasma membrane from the cell cortex (31,32). This process is induced either by contractile force from actomyosin and/or by local rupture of the cortex (31,32). Our results suggest that both phenomena can explain the early stages of polar bleb formation induced by local heating; a temperature gradient increases the contractile force of actomyosin at the warmer side [Fig. 4 *E* (*i*)–(*iii*)] or induces local rupture of the cortex [Fig. 4 *E* (*i*)–(*iii'*)], both of which can trigger the detachment of cortex from the plasma membrane and initiate a polar bleb formation. Subsequently, at the warmer side, the actomyosin contractile force decreases and the cortex ruptures [Fig. 4 *E* (*iv*)], immediately followed by the accumulation of cortex toward the cooler side and extension of the bleb at the warmer side [Fig. 4 *E* (*v*)] (see Discussion below). Under small temperature gradients or uniform heating, the process as shown in (*i*)–(*iii*) or (*i*)–(*iii'*) occurs in many regions, resulting in the formation of multiple non-directional blebs.

Increased contractility model for the initiation of polar bleb formation [Fig. 4 *E* (*ii*)–(*iii*)] is expected by the following observations; after detachment of the plasma membrane from the cell cortex during heating, the shape of the cortex at the warmer side was straightened (10 s in Fig. 4 *A* and Movie S17) and then returned to an arched shape after re-cooling (22.5 s in Fig. 4 *C* and Movie S17). These changes in cortex shape can be explained by the increased contractile force at the warmer side during heating that is analogous to our previous reports on skeletal muscle myosin. We reported that the tension generated on an actin filament by skeletal muscle myosins increases at higher temperature (20) due to increased number of cross bridges (33,34). In this line, it was reported that A549 cells become stiffer at higher temperature (35). Contrary to this report, other groups showed that stiffness and cortical tension decrease at higher temperature (36–40). We noted that the polar bleb was formed even when the cortex was stabilized by jasplakinolide (Fig. 2 *A*), suggesting the increased contractility model as a major route at least in the presence of this drug. Further investigation is desired for temperature dependence of force generation by cortical actomyosin in cells.

During blebbing, the rupture of cortex occurred at the warmer side in most cases [Fig. 4 *E* (*iv*) or (*ii'*)], as observed by the decrease in cortex density (Figs. 3, *A* and *B*, and 4, *A*–*C*). This may occur either through actin network disassembly by the temperature-enhanced contractile force of myosin II (41–44) at the warmer side, or through decreased cortical tension following instantaneous enhancement by heating. Our following observation can be explained by the latter; the density of MRLC was decreased at the warmer side even in the presence of blebbistatin and Y-27632 (Fig. 3 *B*; Movies S12 and S15). This thermal dissociation of myosin II from actin filaments, or MRLC from myosin II molecules, may reduce the contractile force, and destabilise the cortex. This rupture could escalate bleb extension by eliminating the physical barrier for intracellular components (Fig. S14; Movie

S19). The gap created in the cortex seems to be large, as a spindle can move into the polar bleb through the ruptured cortex (Fig. S14; Movie S19). After the polar bleb formation, F-actin re-formed in the bleb (Fig. 4 *A*; Movie S17), which might have contributed to the retraction (Fig. S5 *C*) as in classical blebbing (31,32). In the polar bleb formation induced by temperature gradient, many kinds of other factors could be involved. Thermophoresis has a potential to generate asymmetric distribution of ATP and other molecules. Temperature gradient could break the symmetry of enzyme activities and kinetics of various proteins regulating actin polymerization/depolymerization, stability of cortex, adhesion of cortex-membrane, and force generation by myosin II. To rule in or out the involvement of these factors, bottom-up approach using artificial cell system (i.e., reconstructed actomyosin cortex in liposome) is desired in further studies.

Ca^{2+} increase may affect the structure of actomyosin complexes. For instance, high concentrations of Ca^{2+} induces the formation of dense F-actin networks (45). Ca^{2+}/calmodulin-activated MLCK increases the activity of myosin II (46). To confirm whether Ca^{2+} bursts are involved in the bleb formation, we examined the significance of intracellular Ca^{2+} by applying Ca^{2+} chelators, EGTA-AM and BAPTA-AM [the Ca^{2+} binding rate of BAPTA is ~40 times higher than that of EGTA (47)]. Both intracellular EGTA and BAPTA prevented the Ca^{2+} burst during heating and also after re-cooling under conditions that induce polar blebs (T_0 = 25°C, ΔT = 12°C) (Fig. S10, *B* and *C*). Then, BAPTA-loaded cells show bleb extension similar to non-treated cells, whereas EGTA-loaded cells produced longer bleb extensions (Fig. S10 *D*). This difference between EGTA and BAPTA might be attributable to BAPTA that can depolymerize actin filaments (48), and probably reduce the cortex tension. In overall, these results suggest that Ca^{2+} burst during heating suppresses the extension of polar bleb. In accordance with these observations, the probability of forming multiple blebs decreased with both intracellular EGTA and BAPTA by about a half, probably because decreased intracellular Ca^{2+} concentration reduces force generation of the actomyosin cortex (40,49).

The different effects of Y-27632 (ROCK inhibitor) and ML-7 (MLCK inhibitor) on the formation of a polar bleb (Fig. 2 A) suggest that ROCK-mediated contractile force is mainly involved in the formation of polar blebs induced by local heating, but the contribution of MLCK-mediated force is limited. Y-27632 is known to inhibit osmotic stress-induced blebbing, but ML-7 does not suppress the blebbing (50). Our results are consistent with these observations. Further investigation into spatially distinct phosphorylation of MLC could reveal the more detailed mechanism for actomyosin-based cellular responses to temperature gradient.

Nocodazole (microtubule-depolymerizing drug) significantly increased the length of polar blebs induced by heating, whereas taxol (microtubule stabilizer) did not increase the extension length (Fig. 2 *A*). These results suggest that microtubule structures such as the

mitotic spindle suppress the bleb extension. Supporting this result, in most cases, the spindle did not move into the bleb due to the physical cortex barrier (Fig. S14 *A*; Movie S19). In other cases, however, the spindle moved into the bleb through the gap where the actomyosin cortex was broken (Fig. S14 *B*; Movie S19), and this relocation of spindle led to large bleb formation (Fig. S14 *C*). In addition, the activation of RhoA by nocodazole through microtubule depolymerization (51,52) might also be related to increased extension of the polar bleb induced by heating.

The minimum temperature gradient producing polar blebbing is 1.3°C across the cell (diameter ~20 μm: ≥ ~0.065°C μm^{-1}), equivalent to 50–100°C mm^{-1}. In the best of our knowledge, such a steep temperature gradient has not been observed in a human body. On the other hand, local heating techniques attract attentions as novel non-invasive methods for regulating cell functions (6–13). Furthermore, in advanced thermal therapies of tumor tissues, magnetic or gold nanoparticles are currently used as heat sources in clinical trials (53–59). Considering that each micro- and nano-sized heat source can increase the local temperature up to 46°C and generate a gradient as sharp as 1.3°C within each individual cell, blebs are expected to form in these thermal treatments. Also, our results provide a safeguard for a bleb tension measurement with IR laser previously reported (60). With the estimated temperature increase of 0.02°C during tension measurement (60), IR laser is considered to have a limited effect, if any.

Although local heating for 20 s does not completely kill the cells within 1 h (Fig. S7), even short-pulsed local heating for only 5 s inhibited normal cytokinesis above 46°C (Fig. S8 *A*). Interestingly, trisection was observed in both unheated and heated cells. The cell size before trisection or multisection appeared to be larger than that of divided cells (Fig. S8 *B*), suggesting that these larger cells have a tendency to trisect independent of heating (61). However, even normal-sized cells (33%; 2/6) trisected due to heating (Fig. S8 *B*), indicating that local heating has a potential to induce trisection. We also observed that the spindle appeared disorganized due to mechanical stress at the interface between the cell body and the polar bleb (Fig. S14; Movie S19). These effects from local heating and bleb formation might contribute to the efficiency of thermal therapies.

Author contributions

K.O., T.A., A.I., H.I., M.S., and S.I. designed the research. K.O., M.M., and M.S. developed the optical setup. K.O., T.A., A.I., T.S., and Y.S. performed experiments and analyzed the data under the guidance of M.S. and S.I. Y.S., T.I., and T.O. constructed the plasmids. K.O., T.A., A.I., M.S., and S.I. wrote the manuscript. All authors discussed the results and commented on the manuscript.

Acknowledgements

This research was supported by Research Fellowship for Young Scientists (to K.O.) from Japan Society for the Promotion of Science (JSPS), the Grants-in-Aid for Young Scientist (A) (to K.O and M.S.), Scientific Research on Innovative Areas "Nanomedicine Molecular Science" (No. 2306) (to K.O. and M.S.), Specially Promoted Research (to S.I.), and Scientific Research (S) (to S.I.) from the Ministry of Education, Culture, Sports, Science and Technology (MEXT) of Japan. H.I. was supported by the A*STAR Research Attachment Programme (ARAP) from Singapore's Agency for Science, Technology and Research (A*STAR). The authors declare no competing financial interests.

Supporting Citations

References (62‑69) appear in the Supporting Material.

References

1. Clapham, D.E. 2003. TRP channels as cellular sensors. *Nature*. 426: 517–524.

2. Sakai, T. 1986. Rapid cooling contracture. *Jpn. J. Physiol.* 36: 423–431.

3. Tseeb, V., M. Suzuki, K. Oyama, K. Iwai, and S. Ishiwata. 2009. Highly thermosensitive Ca^{2+} dynamics in a HeLa cell through IP_3 receptors. *HFSP J.* 3: 117–123.

4. Itoh, H., K. Oyama, M. Suzuki, and S. Ishiwata. 2014. Microscopic heat pulse-induced calcium dynamics in single WI-38 fibroblasts. *BIOPHYSICS*. 10: 109–119.

5. Xiao, B., B. Coste, J. Mathur, and A. Patapoutian. 2011. Temperature-dependent STIM1 activation induces Ca^{2+} influx and modulates gene expression. *Nat. Chem. Biol*. 7: 351–358.

6. Huang, H., S. Delikanli, H. Zeng, D.M. Ferkey, and A. Pralle. 2010. Remote control of ion channels and neurons through magnetic-field heating of nanoparticles. *Nat. Nanotechnol.* 5: 602–606.

7. Chen, R., G. Romero, M.G. Christiansen, A. Mohr, and P. Anikeeva. 2015. Wireless magnetothermal deep brain stimulation. *Science*. 347: 1477–1480.

8. Kamei, Y., M. Suzuki, K. Watanabe, K. Fujimori, T. Kawasaki, T. Deguchi, Y. Yoneda, T. Todo, S. Takagi, T. Funatsu, and S. Yuba. 2009. Infrared laser-mediated gene induction in targeted single cells in vivo. *Nat. Methods*. 6: 79–81.

9. Shapiro, M.G., K. Homma, S. Villarreal, C. P. Richter, and F. Bezanilla. 2012. Infrared light excites cells by changing their electrical capacitance. *Nat. Commun*. 3: 736.

10. Liu, Q., M.J. Frerck, H.A. Holman, E.M. Jorgensen, and R.D. Rabbitt. 2014. Exciting cell membranes with a blustering heat shock. *Biophys. J*. 106: 1570–1577.

11. Oyama, K., A. Mizuno, S. A. Shintani, H. Itoh, T. Serizawa, N. Fukuda, M. Suzuki, and S. Ishiwata. 2012. Microscopic heat pulses induce contraction of cardiomyocytes without calcium transients. *Biochem. Biophys. Res. Commun*. 417: 607–612.

12. Miyako, E., J. Russier, M. Mauro, C. Cebrian, H. Yawo, C. Ménard-Moyon, J.A. Hutchison, M. Yudasaka, S. Iijima, L. De Cola, C. Ménard-Moyon, L. De Cola, and A. Bianco. 2014. Photofunctional Nanomodulators for Bioexcitation. *Angew. Chem. Int. Ed. Engl*. 53: 13121–13125.

13. Shintani, S.A., K. Oyama, S. Ishiwata, and N. Fukuda. 2015. High-frequency sarcomeric auto-oscillations induced by heating in living neonatal cardiomyocytes of the rat. *Biochem. Biophys. Res. Commun.* 457: 165–170.

14. Bonner, J.T., W.W. Clarke, C.L. Neely, and M.K. Slifkin. 1950. The orientation to light and the extremely sensitive orientation to temperature gradients in the slime mold Dictyostelium discoideum. *J. Cell. Physiol*. 36: 149–158.

15. Maeda, K., Y. Imae, J.I. Shioi, and F. Oosawa. 1976. Effect of temperature on motility and chemotaxis of Escherichia coli. *J. Bacteriol*. 127: 1039–1046.

16. Bahat, A., I. Tur-Kaspa, A. Gakamsky, L.C. Giojalas, H. Breitbart, and M. Eisenbach. 2003. Thermotaxis of mammalian sperm cells: a potential navigation mechanism in the female genital tract. *Nat. Med*. 9: 149–150.

17. Eisenbach, M., and L.C. Giojalas. 2006. Sperm guidance in mammals － an unpaved road to the egg. *Nat. Rev. Mol. Cell Biol*. 7: 276–285.

18. Pomerance, A., J. Matthews, M. Ferguson, J.S. Urbach, and W. Losert. 2005. Actin polymerization in a thermal gradient. *Macromol Symp*. 227: 231–242.

19. Kakugo, A., Y. Tamura, K. Shikinaka, M. Yoshida, R. Kawamura, H. Furukawa, Y. Osada, and J.P. Gong. 2009. Formation of well-oriented microtubules with preferential polarity in a confined space under a temperature gradient. *J. Am. Chem. Soc*. 131: 18089–18095.

20. Kato, H., T. Nishizaka, T. Iga, K. Kinosita, and S. Ishiwata. 1999. Imaging of thermal activation of actomyosin motors. *Proc. Natl. Acad. Sci. USA*. 96: 9602–9606.

21. Kawaguchi, K., and S. Ishiwata. 2001. Thermal activation of single kinesin molecules with temperature pulse microscopy. *Cell Motil. Cytoskeleton*. 49: 41–47.

22. Iwaki, M., A.H. Iwane, K. Ikezaki, and T. Yanagida. 2015. Local heat activation of single myosins based on optical trapping of gold nanoparticles. *Nano Lett.* 15: 2456–2461.

23. Duhr, S., and D. Braun. 2006. Why molecules move along a temperature gradient. *Proc. Natl. Acad. Sci. USA*. 103: 19678–19682.

24. Maeda, Y.T., A. Buguin, and A. Libchaber. 2011. Thermal separation: interplay between the Soret effect and entropic force gradient. *Phys. Rev. Lett*. 107: 038301.

25. Oyama, K., M. Takabayashi, Y. Takei, S. Arai, S. Takeoka, S. Ishiwata, and M. Suzuki. 2012. Walking nanothermometers: spatiotemporal temperature measurement of transported acidic organelles in single living cells. *Lab Chip*. 12: 1591–1593.

26. Reichl, M.R., and D. Braun. 2014. Thermophoretic manipulation of molecules inside living cells. *J. Am. Chem. Soc*. 136: 15955–15960.

27. Zeeb, V., M. Suzuki, and S. Ishiwata. 2004. A novel method of thermal activation and temperature measurement in the microscopic region around single living cells. *J. Neurosci. Methods*. 139: 69–77.

28. Riedl, J., A.H. Crevenna, K. Kessenbrock, J.H. Yu, D. Neukirchen, M. Bista, F. Bradke, D. Jenne, T. A. Holak, Z. Werb, M. Sixt, and R. Wedlich-Soldner. 2008. Lifeact: a versatile marker to visualize F-actin. *Nat. Methods*. 5: 605–607.

29. Lecuit, T., and P. F. Lenne. 2007. Cell surface mechanics and the control of cell shape, tissue patterns and morphogenesis. *Nat. Rev. Mol. Cell Biol*. 8: 633–644.

30. Clark, A.G., and E. Paluch. 2011. Mechanics and regulation of cell shape during the cell cycle. *Results Probl. Cell Differ*. 53: 31–73.

31. Charras, G., and E. Paluch. 2008. Blebs lead the way: how to migrate without lamellipodia. *Nat. Rev. Mol. Cell Biol*. 9: 730–736.

32. Paluch, E.K., and E. Raz. 2013. The role and regulation of blebs in cell migration. *Curr. Opin. Cell Biol*. 25: 582–590.

33. Kawai, M., K. Kawaguchi, M. Saito, and S. Ishiwata. 2000. Temperature change does not affect force between single actin filaments and HMM from rabbit muscles. *Biophys. J.* 78: 3112–3119.

34. Kawai, M., T. Kido, M. Vogel, R.H.A. Fink, and S. Ishiwata. 2006. Temperature change does not affect force between regulated actin filaments and heavy meromyosin in single-molecule experiments. *J. Physiol.* 574: 877–887.

35. Sunyer, R., X. Trepat, J.J. Fredberg, R. Farré, and D. Navajas. 2009. The temperature dependence of cell mechanics measured by atomic force microscopy. *Phys. Biol.* 6: 025009.

36. Williamson, J.R., M.O. Shanahan, and R.M. Hochmuth. 1975. The influence of temperature on red cell deformability. *Blood.* 46: 611–624.

37. Petersen, N.O., W.B. McConnaughey, and E.L. Elson. 1982. Dependence of locally measured cellular deformability on position on the cell, temperature, and cytochalasin B. *Proc. Natl. Acad. Sci. U. S. A.* 79: 5327–5331.

38. Liu, B., C.J. Goergen, and J.-Y. Shao. 2007. Effect of temperature on tether extraction, surface protrusion, and cortical tension of human neutrophils. *Biophys. J.* 93: 2923–2933.

39. Rico, F., C. Chu, M.H. Abdulreda, Y. Qin, and V.T. Moy. 2010. Temperature modulation of integrin-mediated cell adhesion. *Biophys. J.* 99: 1387–1396.

40. Chan, C.J., G. Whyte, L. Boyde, G. Salbreux, and J. Guck. 2014. Impact of heating on passive and active biomechanics of suspended cells. *Interface Focus.* 4: 20130069.

41. Haviv, L., D. Gillo, F. Backouche, and A. Bernheim-Groswasser. 2008. A cytoskeletal demolition worker: myosin II acts as an actin depolymerization agent. *J. Mol. Biol*. 375: 325–330.

42. Wilson, C.A., M.A. Tsuchida, G.M. Allen, E.L. Barnhart, K.T. Applegate, P.T. Yam, L. Ji, K. Keren, G. Danuser, and J.A. Theriot. 2010. Myosin II contributes to cell-scale actin network treadmilling through network disassembly. *Nature*. 465: 373–377.

43. Murrell, M.P., and M.L. Gardel. 2012. F-actin buckling coordinates contractility and severing in a biomimetic actomyosin cortex. *Proc. Natl. Acad. Sci. USA.* 109: 20820–20825.

44. Reymann, A.-C., R. Boujemaa-Paterski, J.-L. Martiel, C. Guérin, W. Cao, H.F. Chin, E.M. De La Cruz, M. Théry, and L. Blanchoin. 2012. Actin network architecture can determine myosin motor activity. *Science*. 336: 1310–1314.

45. Jung, S.-R., M.-H. Kim, B. Hille, and D.-S. Koh. 2009. Control of granule mobility and exocytosis by Ca^{2+}-dependent formation of F-actin in pancreatic duct epithelial cells. *Traffic*. 10: 392–410.

46. Matsumura, F. 2005. Regulation of myosin II during cytokinesis in higher eukaryotes. *Trends Cell Biol*. 15: 371–377.

47. Eggermann, E., I. Bucurenciu, S.P. Goswami, and P. Jonas. 2011. Nanodomain coupling between Ca^{2+} channels and sensors of exocytosis at fast mammalian synapses. *Nat. Rev. Neurosci.* 13: 7–21.

48. Saoudi, Y., B. Rousseau, J. Doussière, S. Charrasse, C. Gauthier-Rouvière, N. Morin, C. Sautet-Laugier, E. Denarier, R. Scaïfe, C. Mioskowski, and D. Job. 2004. Calcium-independent cytoskeleton disassembly induced by BAPTA. *Eur. J. Biochem.* 271: 3255–3264.

49. Gyger, M., R. Stange, T.R. Kießling, A. Fritsch, K.B. Kostelnik, A.G. Beck-Sickinger, M. Zink, and J. A. Käs. 2014. Active contractions in single suspended epithelial cells. *Eur. Biophys. J.* 43: 11–23.

50. Barfod, E.T., A.L. Moore, B.G. Van de Graaf, and S.D. Lidofsky. 2011. Myosin light chain kinase and Src control membrane dynamics in volume recovery from cell swelling. *Mol. Biol. Cell*. 22: 634–650.

51. Ren, X.D., W.B. Kiosses, and M.A. Schwartz. 1999. Regulation of the small GTP-binding protein Rho by cell adhesion and the cytoskeleton. *EMBO J.* 18: 578–585.

52. Norman, L., K. Sengupta, and H. Aranda-Espinoza. 2011. Blebbing dynamics during endothelial cell spreading. *Eur. J. Cell Biol*. 90: 37–48.

53. Johannsen, M., U. Gneveckow, L. Eckelt, A. Feussner, N. Waldöfner, R. Scholz, S. Deger, P. Wust, S. A. Loening, and A. Jordan. 2005. Clinical hyperthermia of prostate cancer using magnetic nanoparticles: Presentation of a new interstitial technique. *Int. J. Hyperthermia*. 21: 637–647.

54. Johannsen, M., U. Gneveckow, K. Taymoorian, B. Thiesen, N. Waldöfner, R. Scholz, K. Jung, A. Jordan, P. Wust, and S. A. Loening. 2007. Morbidity and quality of life during thermotherapy using magnetic nanoparticles in locally recurrent prostate cancer: results of a prospective phase I trial. *Int. J. Hyperthermia*. 23: 315–323.

55. Johannsen, M., U. Gneveckow, B. Thiesen, K. Taymoorian, C.H. Cho, N. Waldöfner, R. Scholz, A. Jordan, S. A. Loening, and P. Wust. 2007. Thermotherapy of prostate cancer using magnetic nanoparticles: feasibility, imaging, and three-dimensional temperature distribution. *Eur. Urol*. 52: 1653–1661.

56. Maier-Hauff, K., F. Ulrich, D. Nestler, H. Niehoff, P. Wust, B. Thiesen, H. Orawa, V. Budach, and A. Jordan. 2011. Efficacy and safety of intratumoral thermotherapy using magnetic iron-oxide nanoparticles combined with external beam radiotherapy on patients with recurrent glioblastoma multiforme. *J. Neurooncol*. 103: 317–324.

57. Wust, P., U. Gneveckow, M. Johannsen, D. Böhmer, T. Henkel, F. Kahmann, J. Sehouli, R. Felix, J. Ricke, and A. Jordan. 2006. Magnetic nanoparticles for interstitial thermotherapy--feasibility, tolerance and achieved temperatures. *Int. J. Hyperthermia*. 22: 673–685.

58. van Landeghem, F.K.H., K. Maier-Hauff, A. Jordan, K.T. Hoffmann, U. Gneveckow, R. Scholz, B. Thiesen, W. Brück, and von Deimling, A. 2009. Post-mortem studies in glioblastoma patients treated with thermotherapy using magnetic nanoparticles. *Biomaterials*. 30: 52–57.

59. Weintraub, K. 2013. Biomedicine: The new gold standard. *Nature*. 495: S14–S16.

60. Peukes, J., and T. Betz. 2014. Direct measurement of the cortical tension during the growth of membrane blebs. *Biophys. J.* 107: 1810–1820.

61. Kiraly, G., G. Nagy, M. Turani, and G. Banfalvi. 2014. Tumor cell fusion and multipolar trivision. *J. Cancer Res. Ther. Oncol*. 2: 1–5.

62. Kapiszewska, M., and L.E. Hopwood. 1986. Changes in bleb formation following hyperthermia treatment of Chinese hamster ovary cells. *Radiat. Res*. 105: 405–412.

63. Sakamoto, T., J. Limouze, C.A. Combs, A.F. Straight, and J.R. Sellers. 2005. Blebbistatin, a myosin II inhibitor, is photoinactivated by blue light. *Biochemistry*. 44: 584–588.

64. Andersen, T., A. Bahadori, D. Ott, A. Kyrsting, S.N.S. Reihani, and P.M. Bendix. 2014. Nanoscale phase behavior on flat and curved membranes. *Nanotechnology*. 25: 505101.

65. Johnson, S.A., B.M. Stinson, M.S. Go, L.M. Carmona, J.I. Reminick, X. Fang, and T. Baumgart. 2010. Temperature-dependent phase behavior and protein partitioning in giant plasma membrane vesicles. *Biochim. Biophys. Acta*. 1798: 1427–1435.

66. Hazel, J.R. 1995. Thermal adaptation in biological membranes: is homeoviscous adaptation the explanation? *Annu. Rev. Physiol*. 57: 19–42.

67. Jackson, W.M., J. Kostyla, J.H. Nordin, and J.F. Brandts. 1973. Calorimetric study of protein transitions in human erythrocyte ghosts. *Biochemistry*. 12: 3662–3667.

68. Brandts, J.F., L. Erickson, K. Lysko, A.T. Schwartz, and R.D. Taverna. 1977. Calorimetric studies of the structural transitions of the human erythrocyte membrane. The involvement of spectrin in the A transition. *Biochemistry*. 16: 3450–3454.

69. Brandts, J.F., R.D. Taverna, E. Sadasivan, and K.A. Lysko. 1978. Calorimetric studies of the structural transitions of the human erythrocyte membrane. Studies of the B and C transitions. *Biochim. Biophys. Acta*. 512: 566–578.

Figure legends

FIGURE 1 Directional blebs formed under temperature gradient in mitotic HeLa cells. (*A*) Schematic illustration of a local heating system. (*B*) Various temperature gradients generated by different laser powers. The heat source indicates the position IR laser was focused. The gradients were measured with TMR-dextran. T_0 = 25°C. (*C*) Schematic illustration of the definition of temperature increase (ΔT) and 'temperature difference' between both sides of a cell. ΔT is defined as the maximum temperature increase in a cell, i.e. the temperature increase at the side of cells near the heat source. (*D*) Sequence of bright-field images showing polar bleb formation induced by local heating (ΔT = 13°C) at T_0 = 37°C (from Movie S1). (*E*) Sequence of bright-field images showing multiple blebs induced by local heating (ΔT = 13°C) at T_0 = 37°C (from Movie S5). (*F*) Sequence of bright-field images showing 'Motionless' induced by strong heating (ΔT = 19°C) at T_0 = 37°C (from Movie S7). Arrowheads indicate the positions of a representative granule. The movement of the granule stopped after heating. Scale bars in (*D–F*), 10 μm. Yellow circles indicate the positions of the heat source. Heating continued for 20 s starting at t = 0 s (red bars). (*G–J*) The relationship between cell reaction and temperature difference between sides of a cell. T_0 = 37°C. A closed yellow circle in (*J*) indicates the formation of multiple blebs induced by uniform heating (Fig. S5 *D*).

FIGURE 2 Effect of inhibitors on bleb formation. (*A*) Extension length in the presence of chemical agents (from Movie S8). From left; Non-treated cells (NT), 0.25% DMSO, 10 μM nocodazole (Noco), 20 μM taxol (Tax), 100 μM blebbistatin (Blebbi), 10 μM Y-27632, 50 μM ML-7, 50 nM jasplakinolide (Jasplak), 10 μM cytochalasin D (Cyto D), and 500 nM latrunculin B (Lat B). The extension length of chemically treated cells was compared to non-treated (NT) cells using Wilcoxon/Mann-Whitney test (*p < 0.05, **p < 0.01, ***p < 0.001; NS, not significant). The extension length in the presence of latrunculin B could not be determined because the response was different from a typical polar bleb formation (see Movie S8). (*B*) The probability of forming multiple blebs in the presence of chemical agents. The concentrations of chemical agents were the same as in (*A*) except for 20 μM ML-7. The multiple blebs were again inhibited by blebbistatin and cytochalasin D, indicating that actomyosin is responsible for the initiation of multiple blebs as for polar bleb. The probability of chemically treated cells was compared to non-treated (NT) cells using Fisher's exact test (**p < 0.01, ***p < 0.001; NS, not significant). (*C*) Probability of 'Motionless' in the presence of chemical agents. 'Motionless' occurred regardless of the presence of 10 μM nocodazole, 100 μM blebbistatin, or 10 μM cytochalasin D.

FIGURE 3 Temperature gradient causes symmetry breaking of the actomyosin cortex. (*A*) Left: image sequences of Lifeact-RFP, actin-RFP, mCherry-MRLC, and CellMask in different cells (created from the original images in Movies S10, S11, S12, S16). Yellow circles indicate the positions of heat sources. Middle: kymographs from the white rectangles in left images. Red bars, the periods of heating. Right: line profiles of fluorescence intensities averaged along white rectangles in the left images before (blue) and after heating (red). Scale bars, 10 μm. (*B*) Relative changes in the maximum fluorescence intensity after heating at the near and the far sides of cells from the heat source. Thick horizontal bars indicate the mean. Statistical significance between the near and far sides for each treatment is represented by grouped bars at the top and reported using a paired *t*-test, and the fluorescence intensity at each side is compared to non-treated cells (NT) using a *t*-test (*p < 0.05, **p < 0.01, ***p < 0.001; NS, not significant). ΔT = 15°C, T_0 = 25°C. NT, non-treated. Blebbi, 100 μM blebbistatin. Y-27632, 10 μM Y-27632. Cyto D, 10 μM cytochalasin D.

FIGURE 4 Asymmetric distribution of the actin cortex and plasma membrane in the initiation of a directional polar bleb under temperature gradient. (*A*) Image sequences of fluorescently labelled F-actin (Lifeact-GFP) and plasma membrane (PM) (CellMask) in the same cell (created from the original images of Movie S17). ΔT = 15°C at T_0 = 25°C. Top images are in pseudo-color to highlight the dynamics of Lifeact-GFP. Scale bar, 10 μm. (*B*) Kymographs of Lifeact-GFP (green) and CellMask (magenta), and their merged images from the white rectangles in (*A*). (*C*) Time courses of fluorescence intensities measured at vertical black bars in (*B*). Arrows and red bars in (*A*–*C*) indicate the timing of initiation of bleb formation and the period of heating, respectively. The gray area in (*C*) also indicates the period of heating. The rapid fluorescence decrease at the onset of heating and increase at the end of heating are due to the effect of thermal quenching of fluorophores. In-phase movement of the actin cortex and plasma membrane induced by local heating. (*D*) In-phase movement of the actin cortex and plasma membrane to the cooler side. These sequences were reconstructed from the polar transformed images of (*A*). Vertical red bars indicate the period of heating. Angle is defined as relative to the heat source (see Fig. S2: the position at 0° is the nearest to the heat source), and negative value is defined as the counter-clockwise direction. See also Fig. S11. (*E*) Schematic model on the initiation of directional bleb formation by local heating. A possible '*Major case 1*': (*i*), (*ii*), Local heating increases the contractile forces (orange arrows) more at the warmer side. (*iii*), The increased force at the warmer side detaches the cortex from the plasma membrane (PM) and the bleb formation begins. (*iv*), While the cortex is ruptured at the warmer side, the bleb continues to extend. (*v*), The cortex rupture results in the movement of the cortex and PM toward the cooler side (green arrows). A possible '*Major case 2*': Cortex ruptures at the warmer side (*ii'*), initiating the bleb formation (*iii'*). A possible '*Minor case*': In a small number of cases, the process

stops at stage (*iii*), where cortex rupture is not observed (Fig. S14; Movie S18). Yellow circles indicate the positions of the heat source.

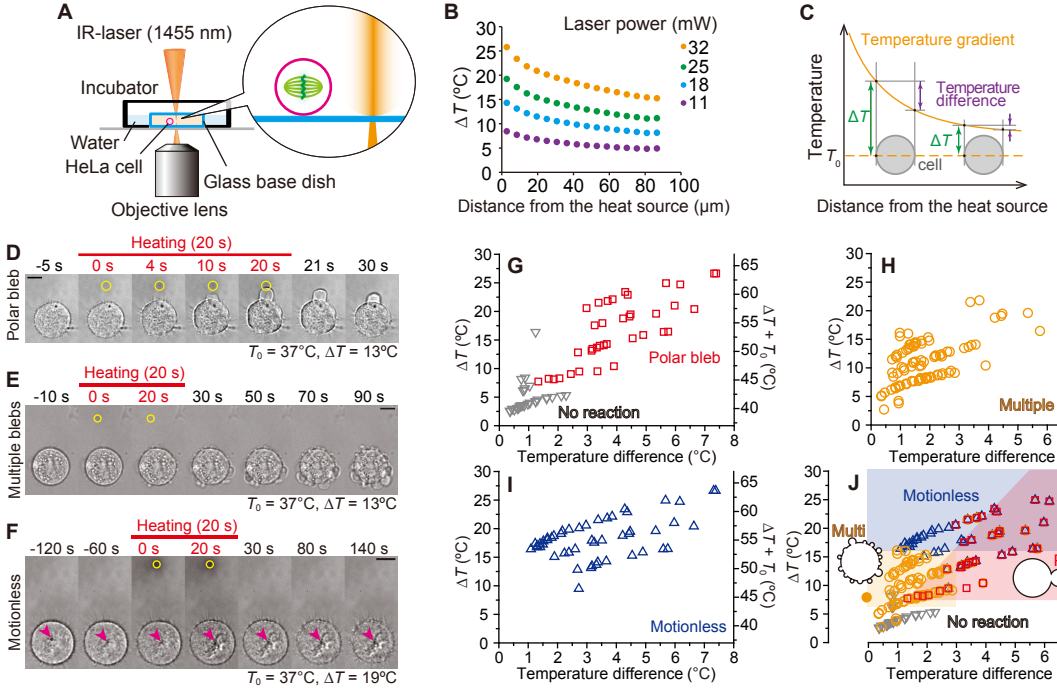
A
IR-laser (1455 nm)
Incubator
Water
HeLa cell
Glass base dish
Objective lens
B
Laser power (mW)
32
25
18
11
ΔT (°C)
Distance from the heat source (μm)
C
Temperature gradient
Temperature
Temperature difference
ΔT
T0
cell
Distance from the heat source
D
Heating (20 s)
-5 s
0 s
4 s
10 s
20 s
21 s
30 s
Polar bleb
T0 = 37°C, ΔT = 13ºC
E
Heating (20 s)
-10 s
0 s
20 s
30 s
50 s
70 s
90 s
Multiple blebs
T0 = 37°C, ΔT = 13ºC
F
Heating (20 s)
-120 s
-60 s
0 s
20 s
30 s
80 s
140 s
Motionless
T0 = 37°C, ΔT = 19ºC
G
Polar bleb
No reaction
ΔT (°C)
ΔT + T0 (°C)
Temperature difference (°C)
H
Multiple blebs
ΔT (°C)
ΔT + T0 (°C)
Temperature difference (°C)
I
Motionless
ΔT (°C)
ΔT + T0 (°C)
Temperature difference (°C)
J
Motionless
Multi
Polar
No reaction
ΔT (°C)
ΔT + T0 (°C)
Temperature difference (°C)

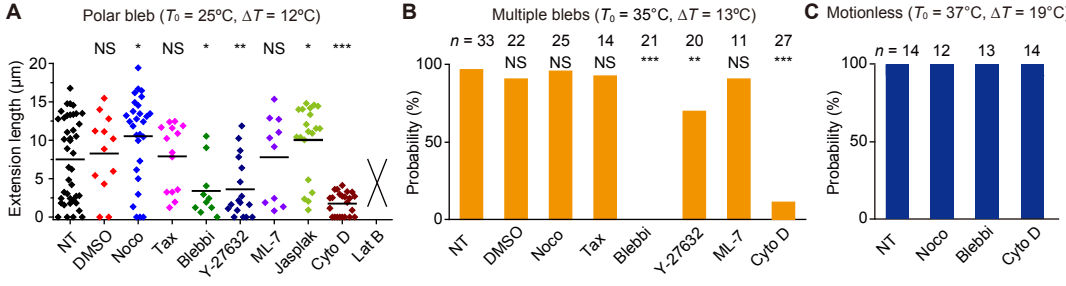
A
Polar bleb (T_0 = 25°C, ΔT = 12°C)
Extension length (μm)
NS * NS * ** NS * ***
NT
DMSO
Noco
Tax
Blebbi
Y-27632
ML-7
Jasplak
Cyto D
Lat B
B
Multiple blebs (T_0 = 35°C, ΔT = 13°C)
Probability (%)
n = 33 22 25 14 21 20 11 27
NS NS NS *** ** NS ***
NT
DMSO
Noco
Tax
Blebbi
Y-27632
ML-7
Cyto D
C
Motionless (T_0 = 37°C, ΔT = 19°C)
Probability (%)
n = 14 12 13 14
NT
Noco
Blebbi
Cyto D

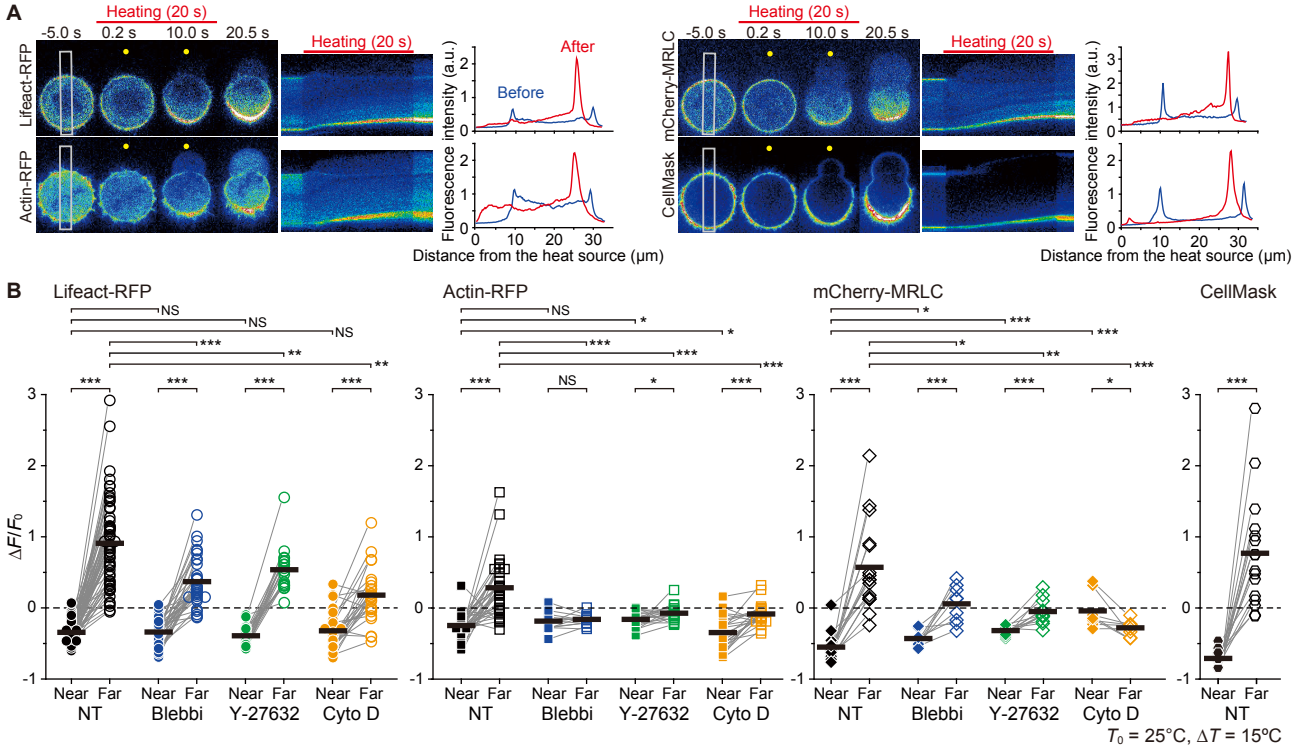
A
Heating (20 s)
-5.0 s
0.2 s
10.0 s
20.5 s
Lifeact-RFP
Actin-RFP
Heating (20 s)
After
Before
Fluorescence intensity (a.u.)
Distance from the heat source (μm)
Heating (20 s)
-5.0 s
0.2 s
10.0 s
20.5 s
mCherry-MRLC
CellMask
Heating (20 s)
Fluorescence intensity (a.u.)
Distance from the heat source (μm)
B
Lifeact-RFP
Actin-RFP
mCherry-MRLC
CellMask
NS
*
**
***
ΔF/F0
Near Far
NT
Blebbi
Y-27632
Cyto D
T0 = 25°C, ΔT = 15°C

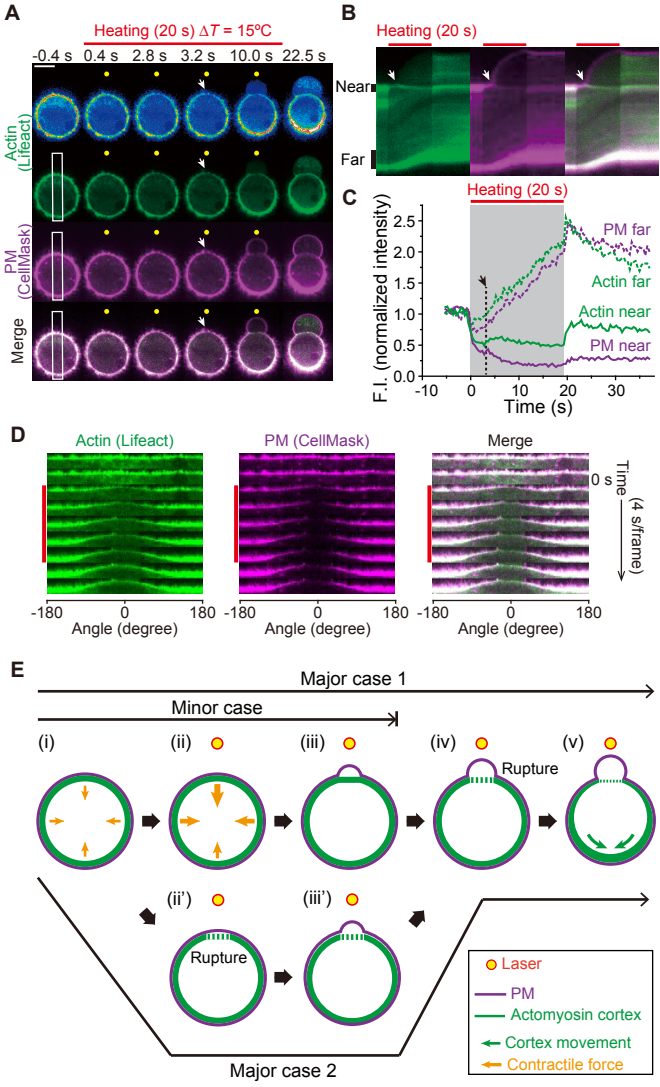
A
Heating (20 s) ΔT = 15ºC
-0.4 s
0.4 s
2.8 s
3.2 s
10.0 s
22.5 s
Actin (Lifeact)
PM (CellMask)
Merge
B
Heating (20 s)
Near
Far
C
Heating (20 s)
F.I. (normalized intensity)
Time (s)
PM far
Actin far
Actin near
PM near
D
Actin (Lifeact)
PM (CellMask)
Merge
Time (4 s/frame)
0 s
Angle (degree)
E
Major case 1
Minor case
(i)
(ii)
(iii)
(iv)
(v)
Rupture
(ii')
(iii')
Rupture
Major case 2
Laser
PM
Actomyosin cortex
Cortex movement
Contractile force